HHS Public Access

Author manuscript

Biochim Biophys Acta. Author manuscript; available in PMC 2019 June 01.

Published in final edited form as:

Biochim Biophys Acta. 2018 June ; 1860(6): 1403–1413. doi:10.1016/j.bbamem.2018.03.030.

Effect of dietary docosahexaenoic acid on rhodopsin content and packing in photoreceptor cell membranes

Subhadip Senapati[1], **Megan Gragg**[1], **Ivy S. Samuels**[2,3], **Vipul M. Parmar**[1], **Akiko Maeda**[1], and **Paul S.–H. Park**[1,*]

[1]Department of Ophthalmology and Visual Sciences, Case Western Reserve University, Cleveland, OH 44106

[2]Research Service, Louis Stokes Cleveland Veterans Administration Medical Center, Cleveland, OH 44106

[3]Department of Ophthalmic Research, Cole Eye Institute, Cleveland Clinic, Cleveland, OH 44195

Abstract

Docosahexaenoic acid (DHA) is enriched in photoreceptor cell membranes. DHA deficiency impairs vision due to photoreceptor cell dysfunction, which is caused, at least in part, by reduced activity of rhodopsin, the light receptor that initiates phototransduction. It is unclear how the depletion of membrane DHA impacts the structural properties of rhodopsin and, in turn, its activity. Atomic force microscopy (AFM) was used to assess the impact of DHA deficiency on membrane structure and rhodopsin organization. AFM revealed that signaling impairment in photoreceptor cells is independent of the oligomeric status of rhodopsin and causes adaptations in photoreceptor cells where the content and density of rhodopsin in the membrane is increased. Functional and structural changes caused by DHA deficiency were reversible.

Graphical Abstract

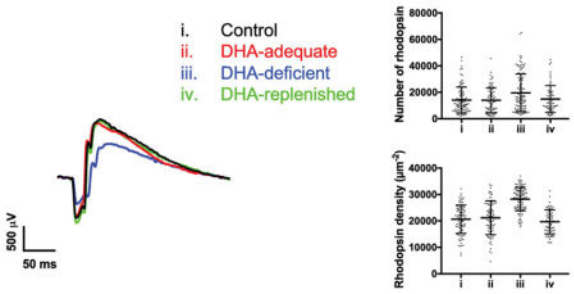

*To whom correspondence should be addressed: Paul S.-H. Park, Department of Ophthalmology and Visual Sciences, Case Western Reserve University, Cleveland, OH 44106, USA, Ph: +1-216-368-2533; Fax: +1-216-368-3171; paul.park@case.edu.

Conflict of interest

All authors declare no conflict of interests exist.

Keywords

G protein-coupled receptor; phospholipid; membrane protein; photoreceptor cell; phototransduction; retina

1. Introduction

Docosahexaenoic acid (DHA) is an essential ω-3 polyunsaturated fatty acid enriched in the brain, testis, and retina [1]. Photoreceptor cells, the light-sensing cells in the outer retina that initiate vision, contain more DHA than any other cell in the body [2–5]. The DHA in photoreceptor cells is incorporated at high levels in the membrane of rod outer segment (ROS) discs [6]. ROS disc membranes are the site of the initial events of vision, where the light receptor rhodopsin initiates phototransduction upon activation by light [7].

Animals cannot synthesize DHA *de novo* and must therefore obtain this essential fatty acid from the diet [8]. Dietary DHA deficiency has been shown to cause vision problems in humans, mice, rats, guinea pigs, and monkeys [9–15]. The vision deficits occur in photoreceptor cells and are related to DHA levels in the membrane [9]. While the detrimental impact of DHA deficiency on photoreceptor cell function has been established [16], the mechanism underlying the defect is unclear. At least some of the functional effects can be attributed to rhodopsin, which is embedded at high concentrations in the ROS disc membranes. DHA in the membrane can bind rhodopsin directly and changes in the amount of DHA can alter the physical properties of the membrane and significantly impact the functional properties of rhodopsin [17–26]. In addition, membrane DHA is predicted to modulate the tertiary and quaternary structures of rhodopsin [21, 27, 28]. Some of the functional deficits may also result from photoreceptor cell loss or disorganization of ROS disc structure [29–31].

To better understand the effect DHA has on the structure of ROS discs and the packing of rhodopsin within the membrane, atomic force microscopy (AFM) was utilized. AFM is an ideal tool to image native biological membranes with high resolution under physiological buffer conditions [32]. ROS disc membranes have been imaged using AFM to reveal the organization of oligomeric rhodopsin into nanoscale domains (i.e., nanodomains) [33–36]. The ability to directly monitor the structure of photoreceptor cell membranes and the packing of rhodopsin within those membranes by AFM has revealed the adaptations of photoreceptor cells to changes in rhodopsin expression and environmental lighting conditions [37, 38]. In the current study, AFM was used to assess the changes in photoreceptor cell membranes and rhodopsin packing that accompany changes in DHA levels in the membrane.

2. Materials and methods

2.1 Animals and diets

C57BL/6J mice (The Jackson Laboratory, Bar Harbor, ME) were used in this study. Mice are normally fed Prolab 3000 diet from LabDiet (St. Louis, MO) in our animal facilities. ROS disc membranes previously investigated by AFM were obtained from mice fed this diet [35,

37, 38]. To establish DHA-deficient and DHA-adequate mouse lines, three generations of mice were fed an ω-3-deficient or ω-3-adequate diets, respectively, and the established lines were maintained on the respective diets. Details about the formulation of the ω-3-deficient and ω-3-adequate diets were described previously and were purchased from Dyets (Bethlehem, PA) [39]. These diets have been shown to modulate the level of DHA in ROS membranes and affect the functional properties of rhodopsin [18]. To determine the reversibility of effects associated with DHA deficiency, DHA-replenished mice were established by feeding 3-week-old DHA-deficient mice the DHA-adequate diet for 4 weeks. All mice were housed under cyclic lighting conditions (12 h dark/12 h light cycle) and were sacrificed after overnight dark adaptation for experiments.

2.2 AFM Imaging and Analysis

All experimental procedures were conducted under dim red light conditions. ROS disc membranes were prepared from 12–15 dark-adapted mice as reported previously [40–42]. Samples were prepared from mice that were 6 weeks of age except for those prepared from DHA-replenished mice, which were 7 weeks of age. 2–3 ROS disc membrane preparations were tested by AFM for each mouse line. Samples were prepared on mica and imaged by AFM as described previously [35, 37]. Contact mode AFM imaging was performed using a Multimode II atomic force microscope equipped with an E scanner (13 μm scan size) and silicon nitride cantilevers with a nominal spring constant of 0.06 N/m (DNP-S, Bruker, Santa Barbara, CA). Deflection images were analyzed using SPIP (version 6.5, Image Metrology A/S, Hørsholm, Denmark), as described previously [37]. Data were plotted and statistical analyses conducted using Prism 6 (GraphPad Software, La Jolla, CA). Statistical significance was determined by one-way ANOVA and Tukey's post-hoc test analysis or by t-test.

2.3 Retinoid analysis

Extraction, derivatization, and separation of retinoids by high-performance liquid chromatography (HPLC) were performed on mouse eye samples as described previously [38, 43]. All reactions involving retinoids were carried out under dim red light. Specific retinoid peaks were identified by their respective elution times and peak wavelength absorbance. Each sample consisted of retinoids extracted from two mouse eyes and 3–5 samples were used for analysis.

2.4 Electroretinography (ERG)

After overnight dark adaptation, mice were anesthetized with 65 mg/kg pentobarbital sodium, the cornea was anesthetized with 1% proparacaine hydrochloride, and the pupils were dilated with 1% tropicamide (Bausch and Lomb, Tampa, FL, USA), 2.5% phenylephrine hydrochloride (Akorn Inc., Lake Forest, IL, USA), and 1% cyclopentolate (Bausch and Lomb, Tampa, FL, USA). Mice were placed on a temperature-regulated heating pad throughout each recording session. Responses of the outer retina were recorded using an Espion E3 ColorDome full-field ganzfeld (Diagnosys, Lowell, MA) with Ag-AgCl cornea electrodes referenced to a Ag-AgCl pellet electrode placed in the mouth of the mouse. For scotopic ERG, ten steps of white light flash stimulus [−3.6 to 2.1 log candela (cd)·s/m^2] were presented in the dark in order of increasing flash strength, and the number of

successive trials averaged together decreased from 20 for low-luminance flashes to 2 for the highest flash stimuli. The duration of the interstimulus interval increased from 4 s for low-luminance flashes to 90 s for the highest flash stimuli. The amplitude of the a-wave was measured 8.3 ms after flash onset from the prestimulus baseline. The amplitude of the b-wave was measured from the a-wave amplitude at 8.3 ms to the peak of the b-wave.

Immediately following the dark-adapted strobe-flash stimuli, the c-wave, generated by the retinal pigment epithelium (RPE), was recorded in response to a 5 cd/m^2 stimulus presented for 30 s. The amplitude of the c-wave was measured from the prestimulus baseline to the peak of the waveform. Immediately after the conclusion of the c-wave recording, a steady 20 cd/m^2 adapting field was presented in the ganzfeld bowl. After 7 min of light adaptation, photopic ERG recordings were obtained from strobe-flash stimuli (−1 to 2 log cd·s/m^2) superimposed on the adapting field. The amplitude of the b-wave was measured from the prestimulus baseline to the positive peak of the waveform.

The a-wave from scotopic ERG traces were analyzed to examine the activity of rod photoreceptor cells. The leading edge of the a-wave (e.g., Fig. 1B) obtained in response to a flash stimulus of 24.1 cd·s/m^2 was analyzed by Eq. 1, a modified form of the Lamb-Pugh model of rod phototransduction [44–46]:

$$P3 = (1 - \exp(-i \cdot S \cdot (t - t_d)^2)) \cdot Rm_{P3} \quad (1)$$

P3 represents the massed response of rod photoreceptor cells and is analogous to Granit's PIII component [47]. The amplitude of *P3* is expressed as a function of flash energy (*i*) and time (*t*) after flash onset. *S* is a sensitivity parameter and is a measure of the gain of phototransduction [44]. Rm_{P3} is the maximum a-wave response and t_d is a brief delay.

Luminance response curves were generated by plotting the amplitude of the b-wave as a function of the first 6 flash intensities of the ERG protocol. These data were fitted with the Naka-Rushton equation (Eq. 2):

$$R/R_{max} = I^n/(I^n + K^n) \quad (2)$$

R is the amplitude of the b-wave at a given flash stimulus luminance (*I*) and R_{max} is the maximum amplitude achieved at a saturating luminance. *K* represents the flash luminance that generates a half-maximal response and *n* is a dimensionless constant that indicates the slope of the function.

Fitting of ERG data to Eq. 1 and Eq. 2 was performed on KaleidaGraph 4 software (Synergy Software, Reading, PA). Statistical significance was determined by one-way ANOVA and Tukey's post-hoc test analysis using Prism 6 (GraphPad Software, La Jolla, CA, USA).

2.5 DHA quantification by mass spectrometry

The DHA standard and the isotope labeled standard DHA-d5 were purchased from Cayman Chemical (Ann Arbor, MI). Retinal tissue or HEK293 cell samples were homogenized in PBS buffer (137 mM NaCl, 2.7 mM KCl, 10 mM Na_2HPO_4, 1.8 mM KH_2PO_4, pH 7.4). A 100 µl aliquot of the homogenate was mixed with 10 µl of internal standard DHA-d5 at a concentration of 2 µg/ml. Phospholipid fatty acids were released by base hydrolysis using 0.2 M NaOH at 60 °C for 30 minutes. Fatty acids were extracted into 4 mL hexane by liquid-liquid extraction. The hexane layer was dried under nitrogen gas and the pellet was resuspended in 100 µl 85% methanol. After centrifugation at 18000 × *g* for 10 min, 50 µl of supernatant was transferred into a vial for DHA analysis by LC-MS-MS. 5 µl of sample was injected into a C18 column (Gemini, 3 µm, 2 × 150 mm, Phenomenex, Torrance, CA) to separate fatty acid species. Mobile phase A was water containing 0.2% acetic acid and mobile phase B was methanol/acetonitrile (1:1) containing 0.2% acetic acid. The pH of the mobile phases was adjusted to 8.0 by ammonium hydroxide. Mobile phase B at 85% was used at 0–2 min, a linear gradient was used starting from 85% to 100% mobile phase B at 2–8 min, and was kept at 100% at 8–20 min at a flow rate of 0.2 ml/min. The eluent was directly injected into a triple quadrupole mass spectrometer (LCMS-8050, Shimadzu, Columbia, MD) and the fatty acids were ionized at ESI negative mode. DHA was quantified using Selected Reaction Monitoring (SRM) and the SRM transitions (m/z) were 327 > 283 for DHA and 332 > 288 for DHA-d5. An internal standard curve was generated using standard DHA at different concentrations with a fixed amount of DHA-d5. The quantity of DHA in the retina tissue was calculated using the internal standard curve. The total protein content in retinal tissue or HEK293 cells was quantified using the Pierce BCA Protein Assay kit (Thermo Fisher Scientific, Waltham, MA).

2.6 Förster resonance energy transfer (FRET) in HEK293 cells

HEK293 cell (HEK293T/17, American Type Culture Collection, Manassas, VA) membranes were enriched with DHA using similar procedures as described previously [48, 49]. HEK293 cells were plated in 12-well plates at a concentration of 150,000 cells/well in Dulbecco's Modified Eagle's Medium (DMEM) - high glucose (Thermo Fisher Scientific, Waltham, MA) supplemented with 10% fetal bovine serum (Thermo Fisher Scientific, Waltham, MA). 4–6 hours after plating, DHA sodium salt (Sigma-Aldrich, St. Louis, MO) from a 100 mM stock solution in ethanol was added to each well to achieve a final concentration of 100 µM. Higher concentrations of DHA sodium salt were toxic to the cells. Cells were transfected the day after plating.

DNA constructs for the expression of opsin tagged with either the yellow fluorescent protein variant SYFP2 or mTurquoise (mTq) were described previously [50, 51]. Procedures for the transfection of HEK293 cells and FRET measurements were also described previously [50, 51]. Briefly, HEK293 cells were cotransfected with different ratios of DNA coding for opsin tagged with SYFP2 or mTq using Lipofectamine 2000 (Invitrogen, Carlsbad, CA). Cells were collected 24 h post-transfection and transferred to a cuvette for FRET measurements. FRET was conducted on a FluoroMax-4 spectrofluorometer (Horiba Jobin Yvon, Edison, NJ). The emission spectra of samples were obtained after exciting mTq at 425 nm. Emission spectra were obtained on untreated cells, cells treated for 5 min with 1.3 mM *n*-dodecyl-β-

D-maltoside (DM, Anatrace, Maumee, OH), and cells treated for 5 min with 3.3 mM SDS (Invitrogen, Carlsbad, CA). The FRET efficiency (E) was computed by measuring the dequenching of the fluorescence signal from mTq (476 nm) upon treatment with detergent. The DM-sensitive E was computed as follows: $E = (mTq_{DM\text{-}treated} - mTq_{untreated})/mTq_{SDS\text{-}treated}$.

2.7 Histology of the retina

Eyes were enucleated from 6-week-old mice and fixed whole in alcoholic Z-fix (Excalibur Pathology, Norma, OK). Eyes were processed, embedded, sectioned and stained by Exacalibur Pathology (Norma, OK). Each eye was placed in a tissue cassette, processed to paraffin on a Sakura VIP 3 tissue processor (Sakura Finetek, Torrance, CA), and embedded with a Reichert-Jung 8040 tissue embedding center (Reichert-Jung, Vienna, Austria). The tissue block was sectioned at 5 μm on an American Optical 820 microtome (American Optical, Buffalo, NY). Ribbons were floated on a water bath (Triangle Biomedical Sciences, Durham, NC) and picked up on glass slides. Slides were air dried overnight and then placed in an oven (68 °C) the next night. Slides were deparaffinized and hydrated to water. Slides were manually stained with Gill 3 Hematoxylin and counterstained with Eosin Y/Phloxine B (StatLab, McKinney, TX). Slides were then dehydrated, cleared, and coverslipped. Retina sections were imaged on a Leica DME compound microscope equipped with an EC3 digital camera and 40×/0.65-NA objective (Leica Microsystems Inc., Buffalo, NY). The length of the ROS was measured at a distance of 200 μm from the optic nerve on the superior side. The number of nuclei spanning the outer nuclear layer was counted manually at various distances from the optic nerve. Data was collected from 4–5 retina sections for each mouse investigated.

3. Results and Discussion

3.1 Dietary DHA deficiency and retinal function

Control mice in the current study were fed the regular diet at our facilities. DHA-adequate and DHA-deficient mouse lines were established by feeding mice the respective diets. Mice were fed DHA-adequate and DHA-deficient diets that were previously characterized in rats [39]. DHA in membrane phospholipids of the retina was quantified by mass spectrometry. DHA-adequate mice exhibited higher levels of DHA in phospholipids of the retina compared to control mice (1.6-fold higher) whereas DHA-deficient mice exhibited lower DHA levels compared to control mice (14 % of levels in control mice) (Tables 1 and S1). The lower levels of DHA could be reversed in DHA-deficient mice by providing those mice with the DHA-adequate diet. After DHA replenishment, mice that were previously DHA deficient exhibited DHA phospholipid levels that were comparable to that in control mice (Tables 1 and S1). Using previously characterized diets, DHA phospholipid levels in the retina of mice were modulated in a comparable manner as that described previously in rats [18, 52].

Previously, *in vitro* studies on ROS membranes from rats fed DHA-adequate and DHA-deficient diets revealed that DHA deficiency results in reduced efficiency in different stages of the phototransduction signaling cascade, including those involving the activation of

rhodopsin and coupling to transducin [18]. These changes appear to underlie changes observed in the physiology of the photoreceptor cells detected by ERG (e.g., [9]). To confirm the effects of DHA deficiency on photoreceptor cell function, ERG was performed. The amplitudes of the a-wave, b-wave, and c-wave, which report the response from photoreceptor cells, bipolar cells, and RPE, respectively [53], were recorded (Fig. 1).

The a-wave and b-wave amplitudes were obtained from ERG traces recorded under scotopic (e.g., Figs. 1A and 1B) and photopic conditions (e.g., 1C). The relationship between the a-wave or b-wave amplitudes and the intensity of the flash stimulus was plotted (Figs. 1D and 1E). The ERG response was similar in control and DHA-adequate mice (Figs. 1A – 1E, Tables S2–S4). In contrast, the ERG response in DHA-deficient mice deviated from that of control and DHA-adequate mice. The scotopic a-wave and b-wave and the photopic b-wave were lower in DHA-deficient mice (Figs. 1D and 1E, Tables S2–S4). The reduction in a-wave and b-wave components of the ERG trace is characteristic of dietary DHA-deficiency [9–11], and points to dysfunction in photoreceptor cells [9].

The leading edge of the scotopic a-wave reflects the cumulative events that take place during phototransduction and correlates with the photocurrent of rod photoreceptor cells [54]. Analysis of the leading edge of the a-wave, evoked by a 24.1 $cd{\cdot}s/m^2$ flash (Fig. 1B), revealed that the sensitivity was lower in DHA-deficient mice compared to that in control or DHA-adequate mice (Tables 2 and S5). The reduced sensitivity is consistent with the reduction in phototransduction efficiency observed in *in vitro* studies on ROS membranes from rats with DHA deficiency [18].

Since bipolar cells receive input from the photoreceptor cells, dysfunction in photoreceptor cell function also alters the luminance response relationship of the b-wave response [55]. Luminance response curves for the scotopic b-wave response were generated and fitted to the Naka-Rushton equation to determine the flash luminance that generates a half-maximal response (K), the maximal b-wave response (R_{max}), and slope factor n. No significant difference in K was observed among control, DHA-adequate, and DHA-deficient mice (Tables 2 and S5). The R_{max} was lower and the slope factor n was higher in DHA-deficient mice compared to that in control or DHA-adequate mice (Tables 2 and S5). The absence of change in K and changes in R_{max} and n indicate that in addition to effects on rod photoreceptor cells, DHA may also impact events occurring downstream of phototransduction in photoreceptor cells such as bipolar cell function [56–58]. Similar effects are also observed when analyzing the luminance response curves of the photopic b-wave response, except no difference was observed for the slope factor n (Tables 2 and S5). Thus, cone photoreceptor cells and their downstream signaling events may also be impacted by DHA deficiency.

As was the case with the a-wave and b-wave, the c-wave amplitude in control and DHA-adequate mice were similar (Fig. 1F, Table S6). The c-wave amplitude in DHA-deficient mice was diminished compared to that in control and DHA-adequate mice (Fig. 1F, Table S6). Since the c-wave amplitude is dependent on the photoreceptor cell response [59], the relationship between the c-wave and a-wave amplitudes was plotted (Fig. 1G). Since the relative ratio between c-wave and a-wave is near 1 (along the dashed line) for DHA-deficient

mice, the decrease in c-wave amplitude is in large part due to a decrease in the a-wave, or photoreceptor cell function. Taken together, DHA-deficiency results in dysfunction in photoreceptor cell function without affecting RPE function. This dysfunction is reversible, however, since DHA-replenished mice exhibit an ERG response similar to that of control and DHA-adequate mice (Fig. 1, Tables 2, S2–S6).

3.2 Impact of DHA on the structure of the retina and ROS

Histology of the retina from control, DHA-adequate, and DHA-deficient mice did not reveal major structural differences (Fig. 2A). The thickness of the outer nuclear layer, assessed by the number nuclei spanning the thickness of this layer, were similar among the different mouse lines (Fig. 2B). Thus, the number of photoreceptor cells in the retina of control, DHA-adequate, and DHA deficient mice were the same and there was no retinal degeneration. The ROS of rod photoreceptor cells were detected in each of the mouse lines, however, the length of the ROS was 17% shorter in DHA-deficient mice compared to that in control or DHA-adequate mice (Fig. 2C). Shortening of the ROS is not predicted to alter the sensitivity or gain of phototransduction [54]. Thus, the altered ERG response observed in DHA-deficient mice are not caused by structural abnormalities of the retina.

The ROS of photoreceptor cells in murine retina contains about 800 stacked membranous discs [60]. Rhodopsin is packed in ROS discs at high concentrations and initiates phototransduction. To determine the effect of modulating membrane DHA levels on ROS disc structure, ROS disc membranes were prepared from each of the different mouse lines and imaged by AFM (Fig. 3). Similar to AFM images of ROS disc membranes reported previously [35–38], ROS disc membranes displayed a characteristic structure of a rim region and lamellar region containing rhodopsin nanodomains, which are formed by oligomeric rhodopsin [33]. Qualitatively, AFM images of ROS disc membranes from the different mouse lines were similar (Fig. 3), which suggests that DHA deficiency does not significantly impact the structure of the ROS disc.

In contrast to diet-induced DHA deficiency examined in the current study, DHA deficiency caused by genetic ablation of proteins required for maintaining membrane DHA levels in photoreceptor cells appears to cause a more severe phenotype that includes retinal degeneration, greater reduction in ROS length, and disorganization of ROS disc structure [29–31]. Thus, DHA deficiency in the membrane of photoreceptor cells caused by diet and genetics are not equivalent. The reason for this difference is unclear. DHA deficiency caused by genetics does not necessarily result in more severe depletion of membrane DHA compared to that caused by diet [29, 30]. Thus, the level of membrane DHA depletion does not appear to be a factor. The proteins required for maintaining membrane DHA levels in photoreceptor cells likely have other functions that are important for photoreceptor cell health.

3.3 Impact of DHA on ROS disc membrane properties and rhodopsin packing

AFM images were analyzed to determine quantitative differences of ROS disc membrane and rhodopsin packing properties (e.g., [37, 38]). ROS disc membrane properties of control mice were first compared to those reported previously under the same conditions [37]. All

ROS disc membrane properties were similar between those determined in the current study and those determined previously (Table S8). This similarity points to the reproducibility of results obtained from our AFM procedures by different users and different preparations.

All mice (control, DHA-adequate, DHA-deficient, and DHA-replenished) displayed similar sized ROS disc membranes (Fig. 4A, Tables 3 and S9). Since the size of ROS disc membranes reflects the diameter of the ROS [38], no change in the diameter of the ROS occurs because of a change in DHA levels. The mean size of rhodopsin nanodomains in ROS disc membranes were similar in all mice (Fig. 4B, Tables 3 and S9). The median size of rhodopsin nanodomains in ROS disc membranes, however, was slightly different for DHA-adequate mice compared to the other mouse lines (Fig. 4C, Tables 3 and S9). DHA-adequate mice had a smaller median nanodomain size compared to the other mice. Despite this small difference, only the median nanodomain size of control and DHA-adequate mice were statistically significant ($p < 0.05$) (Table S9). Since the distribution of nanodomain sizes is skewed [35], the median may be more sensitive to changes compared to the mean. The difference in median nanodomain size of control and DHA-adequate mice may arise from differences in DHA levels (Table 1). Aside from the subtle difference in the size of nanodomains, all other ROS disc membrane properties were the same between control and DHA-adequate mice.

Depletion of DHA in DHA-deficient mice resulted in significant differences in the packing of rhodopsin in ROS disc membranes. Both the number of nanodomains and rhodopsin molecules (Figs. 4D and 4E, Tables 3 and S9) and the density of nanodomains and rhodopsin molecules (Figs. 4F and 4G, Tables 3 and S9) were higher in DHA-deficient mice compared to control and DHA-adequate mice. Estimates of the number of rhodopsin molecules was determined as described previously assuming an oligomeric arrangement within nanodomains [35]. DHA-deficient mice had about 40% more rhodopsin incorporated into the ROS disc membranes compared to either control or DHA-adequate mice (Table 3). To determine whether or not this increase in the packing of rhodopsin in the disc membrane resulted from an increase in protein expression, the amount of rhodopsin in the retina was estimated by quantifying the amount of 11-*cis* retinal in the retina, which is stoichiometric with rhodopsin [61]. Retinoid analysis showed similar levels of 11-*cis* retinal in DHA-deficient mice as in control and DHA-adequate mice (Tables 4 and S10). Thus, the increase in rhodopsin packed into ROS disc membranes of DHA-deficient mice is not a result of increased rhodopsin expression and appears to result in fewer discs, thereby shortening the ROS (Fig. 2C).

Quantification of phospholipid DHA in the retina and ERG analysis indicate that the effects of DHA deficiency are reversible. To test whether or not the effects of DHA deficiency observed in ROS disc membrane properties can be reversed, ROS disc membrane properties of DHA-replenished mice were examined. All properties that were altered in DHA-deficient mice (i.e., number and density of nanodomains and rhodopsin) returned back to values observed in control and DHA-adequate mice when mice were replenished with DHA (Figs. 4D–4G, Tables 3 and S9). Thus, both functional and structural effects of DHA deficiency can be reversed by supplying the diet with an adequate amount of DHA.

3.4 Assessing the effect of DHA deficiency on opsin oligomerization by FRET

Membrane lipids can play important roles in modulating the oligomerization of membrane proteins [62]. ROS disc membranes are unique in that they contain high levels of DHA [2–6]. Under *in vitro* conditions, unsaturated fatty acids with 20–22 carbon atoms favor monomerization of rhodopsin and oligomerization appears to inhibit the activation of rhodopsin [27, 28, 63, 64]. Since DHA is a polyunsaturated fatty acid with 22 carbon atoms, DHA deficiency may further favor oligomerization of rhodopsin, thereby inhibiting rhodopsin activation and reducing the photoreceptor response observed by ERG. Since nanodomains are formed by oligomeric rhodopsin, any change in the oligomeric status of rhodopsin will be reflected in the nanodomain formation and size. The AFM data indicate that the DHA content in ROS disc membranes does not affect the size of nanodomains (Fig. 4, Table 3), which implies that DHA does not modulate rhodopsin oligomerization.

To test the impact of DHA on the oligomerization of rhodopsin in a more direct manner, FRET was utilized to examine the interactions of opsin in HEK293 cells. The level of DHA in the cell membrane was modulated by adding the sodium salt form of the polyunsaturated fatty acid to the media in which the cells are grown. This treatment resulted in a 33-fold increase in the level of DHA (Fig. 5A). FRET was determined at different ratios of mTq- and SYFP2-tagged receptor to determine the maximal FRET efficiency. The maximal FRET efficiency was the same in untreated and DHA-treated cells (Fig. 5B). Thus, the level of DHA in the cell membrane does not affect the oligomeric status of opsin, which contrasts with effects observed in phospholipid vesicles [27, 28]. The oligomeric status of adenosine A_{2A} and dopamine D_2 receptors has also been shown to be independent of the amount of DHA in cell membranes, however, DHA did appear to alter the kinetics of oligomerization [65]. It is unclear whether or not DHA also alters the kinetics of rhodopsin oligomerization without impacting the oligomeric status of the light receptor.

3.5 Origin of rhodopsin packing changes caused by DHA deficiency

From the AFM analysis, it is apparent that DHA deficiency causes significant changes in the packing of rhodopsin in ROS disc membranes. It is unclear, however, whether or not DHA deficiency directly or indirectly causes these changes due to adaptations of the photoreceptor cells in response to perturbed function. Previously, we demonstrated that photostasis effects occur in photoreceptor cells that result in increased rhodopsin density and number [38]. These adaptations occur in response to reduced signaling by the photoreceptor cells, either in the absence of light in constant dark conditions or genetically preventing phototransduction from occurring. To assess whether or not changes observed in DHA-deficient mice are a result of adaptations of the photoreceptor cell due to the reduction in signaling capacity, AFM data from DHA-deficient mice were compared to those from transducin knockout (*Gnat*$^{-/-}$) mice previously published [38].

Gnat$^{-/-}$ mice lack the α-subunit of transducin and therefore signaling is impaired in photoreceptor cells [66]. Interestingly, all the ROS disc membrane parameters of G*nat*$^{-/-}$ mice were found to be similar to those of DHA-deficient mice (Fig. 4, Table S11). No significant differences ($p < 0.05$) were observed in any ROS disc membrane property except for the median size of rhodopsin nanodomains (Table S11). Similar to the case described

earlier comparing control and DHA-adequate mice, the mean nanodomain size was similar between DHA-deficient and G*nat*$^{-/-}$ mice. Thus, any difference in nanodomain size is only modest. This modest difference may be due to differences in the level of DHA in the two mouse lines, where G*nat*$^{-/-}$ mice has comparable levels of DHA as that in control mice (Table 1). Overall, it appears that the impairment of signaling caused by either genetic knockout of transducin or DHA deficiency leads to a similar adaptive response by photoreceptor cells.

Dietary DHA deficiency results in adaptative mechanisms in photoreceptor cells that appear to be initiated to counteract the detected deficiency in signaling. Increased rhodopsin content and density in ROS disc membranes of DHA-deficient mice are achieved in the absence of changes in protein expression. Increased rhodopsin density has been shown previously to result in improved photoreceptor cell function as assessed by ERG [38]. Thus, the increased rhodopsin density observed in DHA-deficient mice indicate that some of the signaling deficiency will be counteracted and that the observed functional deficit is actually less severe than it can be.

4. Conclusions

In the current study, AFM was used to examine the organization of rhodopsin and structure of photoreceptor cell membranes in mice that were fed diets that were either sufficient or deficient in DHA. DHA deficiency resulted in functional defects in photoreceptor cells. The functional defects were not due to disruption of the structure of ROS disc membranes or changes in the oligomeric status of rhodopsin. Rather, the functional defect is likely related to effects that directly impact the function of rhodopsin and signaling partners. DHA deficiency caused by diet appears to differ from those caused by genetics, and the detrimental effects are reversible. Photoreceptor cells can adapt to the dysfunction caused by DHA deficiency to alleviate some of the functional deficit. The observed plasticity in ROS disc membrane properties further demonstrate the adaptability of photoreceptor cells to counteract a variety of effects that can impede vision.

Supplementary Material

Refer to Web version on PubMed Central for supplementary material.

Acknowledgments

We thank Heather Butler and Kathryn Zongolowicz for maintaining mouse colonies. We thank Renliang Zhang in the Proteomics and Metabolomics Laboratory core facility at the Cleveland Clinic Lerner Research Institute (Cleveland, OH) for conducting DHA quantification by mass spectrometry. This work was funded by grants from the National Institutes of Health (R01EY021731 and P30EY011373) and Research to Prevent Blindness (Unrestricted Grant) and a VA Merit Award (I01BX002754).

Abbreviations

AFM	atomic force microscopy
DHA	docosahexaenoic acid

DM	*n*-dodecyl-β-D-maltoside
ERG	electroretinography
FRET	Förster resonance energy transfer
mTq	mTurquoise
HPLC	high-performance liquid chromatography
ROS	rod outer segment(s)
RPE	retinal pigment epithelium

References

1. Lauritzen L, Hansen HS, Jorgensen MH, Michaelsen KF. The essentiality of long chain n-3 fatty acids in relation to development and function of the brain and retina. Prog Lipid Res. 2001; 40:1–94. [PubMed: 11137568]
2. SanGiovanni JP, Chew EY. The role of omega-3 long-chain polyunsaturated fatty acids in health and disease of the retina. Prog Retin Eye Res. 2005; 24:87–138. [PubMed: 15555528]
3. Fliesler SJ, Anderson RE. Chemistry and metabolism of lipids in the vertebrate retina. Prog Lipid Res. 1983; 22:79–131. [PubMed: 6348799]
4. Bazan NG, Molina MF, Gordon WC. Docosahexaenoic acid signalolipidomics in nutrition: significance in aging, neuroinflammation, macular degeneration, Alzheimer's, and other neurodegenerative diseases. Annu Rev Nutr. 2011; 31:321–351. [PubMed: 21756134]
5. Bazan NG. Cell survival matters: docosahexaenoic acid signaling, neuroprotection and photoreceptors. Trends Neurosci. 2006; 29:263–271. [PubMed: 16580739]
6. Boesze-Battaglia K, Albert AD. Fatty acid composition of bovine rod outer segment plasma membrane. Exp Eye Res. 1989; 49:699–701. [PubMed: 2806432]
7. Park PS. Constitutively active rhodopsin and retinal disease. Advances in pharmacology. 2014; 70:1–36. [PubMed: 24931191]
8. Kang JX. Fat-1 transgenic mice: a new model for omega-3 research. Prostaglandins Leukot Essent Fatty Acids. 2007; 77:263–267. [PubMed: 18042365]
9. Benolken RM, Anderson RE, Wheeler TG. Membrane fatty acids associated with the electrical response in visual excitation. Science. 1973; 182:1253–1254. [PubMed: 4752217]
10. Weisinger HS, Vingrys AJ, Bui BV, Sinclair AJ. Effects of dietary n-3 fatty acid deficiency and repletion in the guinea pig retina. Invest Ophthalmol Vis Sci. 1999; 40:327–338. [PubMed: 9950590]
11. Weisinger HS, Vingrys AJ, Sinclair AJ. Effect of dietary n-3 deficiency on the electroretinogram in the guinea pig. Ann Nutr Metab. 1996; 40:91–98. [PubMed: 8773733]
12. Tanito M, Brush RS, Elliott MH, Wicker LD, Henry KR, Anderson RE. High levels of retinal membrane docosahexaenoic acid increase susceptibility to stress-induced degeneration. J Lipid Res. 2009; 50:807–819. [PubMed: 19023138]
13. Neuringer M, Connor WE, Van Petten C, Barstad L. Dietary omega-3 fatty acid deficiency and visual loss in infant rhesus monkeys. J Clin Invest. 1984; 73:272–276. [PubMed: 6317716]
14. Neuringer M, Connor WE, Lin DS, Barstad L, Luck S. Biochemical and functional effects of prenatal and postnatal omega 3 fatty acid deficiency on retina and brain in rhesus monkeys. Proc Natl Acad Sci U S A. 1986; 83:4021–4025. [PubMed: 3459166]
15. Birch DG, Birch EE, Hoffman DR, Uauy RD. Retinal development in very-low-birth-weight infants fed diets differing in omega-3 fatty acids. Invest Ophthalmol Vis Sci. 1992; 33:2365–2376. [PubMed: 1386065]
16. Jeffrey BG, Weisinger HS, Neuringer M, Mitchell DC. The role of docosahexaenoic acid in retinal function. Lipids. 2001; 36:859–871. [PubMed: 11724458]

17. Brown MF. Modulation of rhodopsin function by properties of the membrane bilayer. Chem Phys Lipids. 1994; 73:159–180. [PubMed: 8001180]
18. Niu SL, Mitchell DC, Lim SY, Wen ZM, Kim HY, Salem N Jr, Litman BJ. Reduced G protein-coupled signaling efficiency in retinal rod outer segments in response to n-3 fatty acid deficiency. J Biol Chem. 2004; 279:31098–31104. [PubMed: 15145938]
19. Soubias O, Teague WE, Gawrisch K. Evidence for specificity in lipid-rhodopsin interactions. J Biol Chem. 2006; 281:33233–33241. [PubMed: 16959786]
20. Soubias O, Gawrisch K. Probing specific lipid-protein interaction by saturation transfer difference NMR spectroscopy. J Am Chem Soc. 2005; 127:13110–13111. [PubMed: 16173715]
21. Grossfield A, Feller SE, Pitman MC. A role for direct interactions in the modulation of rhodopsin by omega-3 polyunsaturated lipids. Proc Natl Acad Sci U S A. 2006; 103:4888–4893. [PubMed: 16547139]
22. Bush RA, Malnoe A, Reme CE, Williams TP. Dietary deficiency of N-3 fatty acids alters rhodopsin content and function in the rat retina. Invest Ophthalmol Vis Sci. 1994; 35:91–100. [PubMed: 8300367]
23. Wiedmann TS, Pates RD, Beach JM, Salmon A, Brown MF. Lipid-protein interactions mediate the photochemical function of rhodopsin. Biochemistry. 1988; 27:6469–6474. [PubMed: 3219348]
24. Niu SL, Mitchell DC, Litman BJ. Optimization of receptor-G protein coupling by bilayer lipid composition II: formation of metarhodopsin II-transducin complex. J Biol Chem. 2001; 276:42807–42811. [PubMed: 11544259]
25. Mitchell DC, Niu SL, Litman BJ. Optimization of receptor-G protein coupling by bilayer lipid composition I: kinetics of rhodopsin-transducin binding. J Biol Chem. 2001; 276:42801–42806. [PubMed: 11544258]
26. Sanchez-Martin MJ, Ramon E, Torrent-Burgues J, Garriga P. Improved conformational stability of the visual G protein-coupled receptor rhodopsin by specific interaction with docosahexaenoic acid phospholipid. Chembiochem. 2013; 14:639–644. [PubMed: 23447332]
27. Periole X, Huber T, Marrink SJ, Sakmar TP. G protein-coupled receptors self-assemble in dynamics simulations of model bilayers. J Am Chem Soc. 2007; 129:10126–10132. [PubMed: 17658882]
28. Botelho AV, Huber T, Sakmar TP, Brown MF. Curvature and hydrophobic forces drive oligomerization and modulate activity of rhodopsin in membranes. Biophys J. 2006; 91:4464–4477. [PubMed: 17012328]
29. Rice DS, Calandria JM, Gordon WC, Jun B, Zhou Y, Gelfman CM, Li S, Jin M, Knott EJ, Chang B, Abuin A, Issa T, Potter D, Platt KA, Bazan NG. Adiponectin receptor 1 conserves docosahexaenoic acid and promotes photoreceptor cell survival. Nat Commun. 2015; 6:6228. [PubMed: 25736573]
30. Wong BH, Chan JP, Cazenave-Gassiot A, Poh RW, Foo JC, Galam DL, Ghosh S, Nguyen LN, Barathi VA, Yeo SW, Luu CD, Wenk MR, Silver DL. Mfsd2a Is a Transporter for the Essential omega-3 Fatty Acid Docosahexaenoic Acid (DHA) in Eye and Is Important for Photoreceptor Cell Development. J Biol Chem. 2016; 291:10501–10514. [PubMed: 27008858]
31. Shindou H, Koso H, Sasaki J, Nakanishi H, Sagara H, Nakagawa KM, Takahashi Y, Hishikawa D, Iizuka-Hishikawa Y, Tokumasu F, Noguchi H, Watanabe S, Sasaki T, Shimizu T. Docosahexaenoic acid preserves visual function by maintaining correct disc morphology in retinal photoreceptor cells. J Biol Chem. 2017
32. Whited AM, Park PS. Atomic force microscopy: a multifaceted tool to study membrane proteins and their interactions with ligands. Biochim Biophys Acta. 2014; 1838:56–68. [PubMed: 23603221]
33. Liang Y, Fotiadis D, Filipek S, Saperstein DA, Palczewski K, Engel A. Organization of the G protein-coupled receptors rhodopsin and opsin in native membranes. J Biol Chem. 2003; 278:21655–21662. [PubMed: 12663652]
34. Buzhynskyy N, Salesse C, Scheuring S. Rhodopsin is spatially heterogeneously distributed in rod outer segment disk membranes. J Mol Recognit. 2011; 24:483–489. [PubMed: 21504027]
35. Whited AM, Park PS. Nanodomain organization of rhodopsin in native human and murine rod outer segment disc membranes. Biochim Biophys Acta. 2015; 1848:26–34. [PubMed: 25305340]

36. Rakshit T, Senapati S, Sinha S, Whited AM, Park PSH. Rhodopsin forms nanodomains in rod outer segment disc membranes of the cold-blooded Xenopus laevis. PLoS ONE. 2015; 10:e0141114. [PubMed: 26492040]
37. Rakshit T, Park PS. Impact of reduced rhodopsin expression on the structure of rod outer segment disc membranes. Biochemistry. 2015; 54:2885–2894. [PubMed: 25881629]
38. Rakshit T, Senapati S, Parmar VM, Sahu B, Maeda A, Park PS. Adaptations in rod outer segment disc membranes in response to environmental lighting conditions. Biochim Biophys Acta. 2017; 1864:1691–1702. [PubMed: 28645515]
39. Moriguchi T, Greiner RS, Salem N Jr. Behavioral deficits associated with dietary induction of decreased brain docosahexaenoic acid concentration. J Neurochem. 2000; 75:2563–2573. [PubMed: 11080210]
40. Park PS, Muller DJ. Dynamic single-molecule force spectroscopy of rhodopsin in native membranes. Methods Mol Biol. 2015; 1271:173–185. [PubMed: 25697524]
41. Kawamura S, Colozo AT, Muller DJ, Park PS. Conservation of molecular interactions stabilizing bovine and mouse rhodopsin. Biochemistry. 2010; 49:10412–10420. [PubMed: 21038881]
42. Kawamura S, Colozo AT, Ge L, Muller DJ, Park PS. Structural, energetic, and mechanical perturbations in rhodopsin mutant that causes congenital stationary night blindness. J Biol Chem. 2012; 287:21826–21835. [PubMed: 22549882]
43. Kawamura S, Gerstung M, Colozo AT, Helenius J, Maeda A, Beerenwinkel N, Park PS, Muller DJ. Kinetic, energetic, and mechanical differences between dark-state rhodopsin and opsin. Structure. 2013; 21:426–437. [PubMed: 23434406]
44. Hood DC, Birch DG. Rod phototransduction in retinitis pigmentosa: estimation and interpretation of parameters derived from the rod a-wave. Invest Ophthalmol Vis Sci. 1994; 35:2948–2961. [PubMed: 8206712]
45. Lamb TD, Pugh EN Jr. A quantitative account of the activation steps involved in phototransduction in amphibian photoreceptors. J Physiol. 1992; 449:719–758. [PubMed: 1326052]
46. Pugh EN Jr, Lamb TD. Amplification and kinetics of the activation steps in phototransduction. Biochim Biophys Acta. 1993; 1141:111–149. [PubMed: 8382952]
47. Granit R. The components of the retinal action potential in mammals and their relation to the discharge in the optic nerve. J Physiol. 1933; 77:207–239. [PubMed: 16994385]
48. Mathieu G, Denis S, Langelier B, Denis I, Lavialle M, Vancassel S. DHA enhances the noradrenaline release by SH-SY5Y cells. Neurochem Int. 2010; 56:94–100. [PubMed: 19770016]
49. Champeil-Potokar G, Denis I, Goustard-Langelier B, Alessandri JM, Guesnet P, Lavialle M. Astrocytes in culture require docosahexaenoic acid to restore the n-3/n-6 polyunsaturated fatty acid balance in their membrane phospholipids. J Neurosci Res. 2004; 75:96–106. [PubMed: 14689452]
50. Gragg M, Kim TG, Howell S, Park PS. Wild-type opsin does not aggregate with a misfolded opsin mutant. Biochim Biophys Acta. 2016; 1858:1850–1859. [PubMed: 27117643]
51. Miller LM, Gragg M, Kim TG, Park PS. Misfolded opsin mutants display elevated beta-sheet structure. FEBS Lett. 2015; 589:3119–3125. [PubMed: 26358292]
52. Moriguchi T, Loewke J, Garrison M, Catalan JN, Salem N. Reversal of docosahexaenoic acid deficiency in the rat brain, retina, liver, and serum. J Lipid Res. 2001; 42:419–427. [PubMed: 11254754]
53. Weymouth AE, Vingrys AJ. Rodent electroretinography: methods for extraction and interpretation of rod and cone responses. Prog Retin Eye Res. 2008; 27:1–44. [PubMed: 18042420]
54. Breton ME, Schueller AW, Lamb TD, Pugh EN Jr. Analysis of ERG a-wave amplification and kinetics in terms of the G-protein cascade of phototransduction. Invest Ophthalmol Vis Sci. 1994; 35:295–309. [PubMed: 8300357]
55. Hood DC, Birch DG. A computational model of the amplitude and implicit time of the b-wave of the human ERG. Vis Neurosci. 1992; 8:107–126. [PubMed: 1558823]
56. Evans LS, Peachey NS, Marchese AL. Comparison of three methods of estimating the parameters of the Naka-Rushton equation. Doc Ophthalmol. 1993; 84:19–30. [PubMed: 8223107]

57. Arden GB, Carter RM, Hogg CR, Powell DJ, Ernst WJ, Clover GM, Lyness AL, Quinlan MP. A modified ERG technique and the results obtained in X-linked retinitis pigmentosa. Br J Ophthalmol. 1983; 67:419–430. [PubMed: 6860609]
58. Massof RW, Wu L, Finkelstein D, Perry C, Starr SJ, Johnson MA. Properties of electroretinographic intensity-response functions in retinitis pigmentosa. Doc Ophthalmol. 1984; 57:279–296. [PubMed: 6468246]
59. Samuels IS, Sturgill GM, Grossman GH, Rayborn ME, Hollyfield JG, Peachey NS. Light-evoked responses of the retinal pigment epithelium: changes accompanying photoreceptor loss in the mouse. J Neurophysiol. 2010; 104:391–402. [PubMed: 20484527]
60. Liang Y, Fotiadis D, Maeda T, Maeda A, Modzelewska A, Filipek S, Saperstein DA, Engel A, Palczewski K. Rhodopsin signaling and organization in heterozygote rhodopsin knockout mice. J Biol Chem. 2004; 279:48189–48196. [PubMed: 15337746]
61. Dowling JE. Chemistry of visual adaptation in the rat. Nature. 1960; 188:114–118. [PubMed: 13724150]
62. Gupta K, Donlan JAC, Hopper JTS, Uzdavinys P, Landreh M, Struwe WB, Drew D, Baldwin AJ, Stansfeld PJ, Robinson CV. The role of interfacial lipids in stabilizing membrane protein oligomers. Nature. 2017; 541:421–424. [PubMed: 28077870]
63. Soubias O, Teague WE Jr, Hines KG, Gawrisch K. Rhodopsin/lipid hydrophobic matching-rhodopsin oligomerization and function. Biophys J. 2015; 108:1125–1132. [PubMed: 25762324]
64. Niu SL, Mitchell DC. Effect of packing density on rhodopsin stability and function in polyunsaturated membranes. Biophys J. 2005; 89:1833–1840. [PubMed: 15980173]
65. Guixa-Gonzalez R, Javanainen M, Gomez-Soler M, Cordobilla B, Domingo JC, Sanz F, Pastor M, Ciruela F, Martinez-Seara H, Selent J. Membrane omega-3 fatty acids modulate the oligomerisation kinetics of adenosine A2A and dopamine D2 receptors. Scientific reports. 2016; 6:19839. [PubMed: 26796668]
66. Calvert PD, Krasnoperova NV, Lyubarsky AL, Isayama T, Nicolo M, Kosaras B, Wong G, Gannon KS, Margolskee RF, Sidman RL, Pugh EN Jr, Makino CL, Lem J. Phototransduction in transgenic mice after targeted deletion of the rod transducin alpha -subunit. Proc Natl Acad Sci U S A. 2000; 97:13913–13918. [PubMed: 11095744]

Highlights

- DHA in the membrane of photoreceptor cells was modulated by diet
- DHA deficiency impaired photoreceptor cell function
- DHA deficiency increased rhodopsin content and density in the membrane
- DHA deficiency did not alter rhodopsin oligomerization or disc membrane structure
- Effects of DHA deficiency were reversible

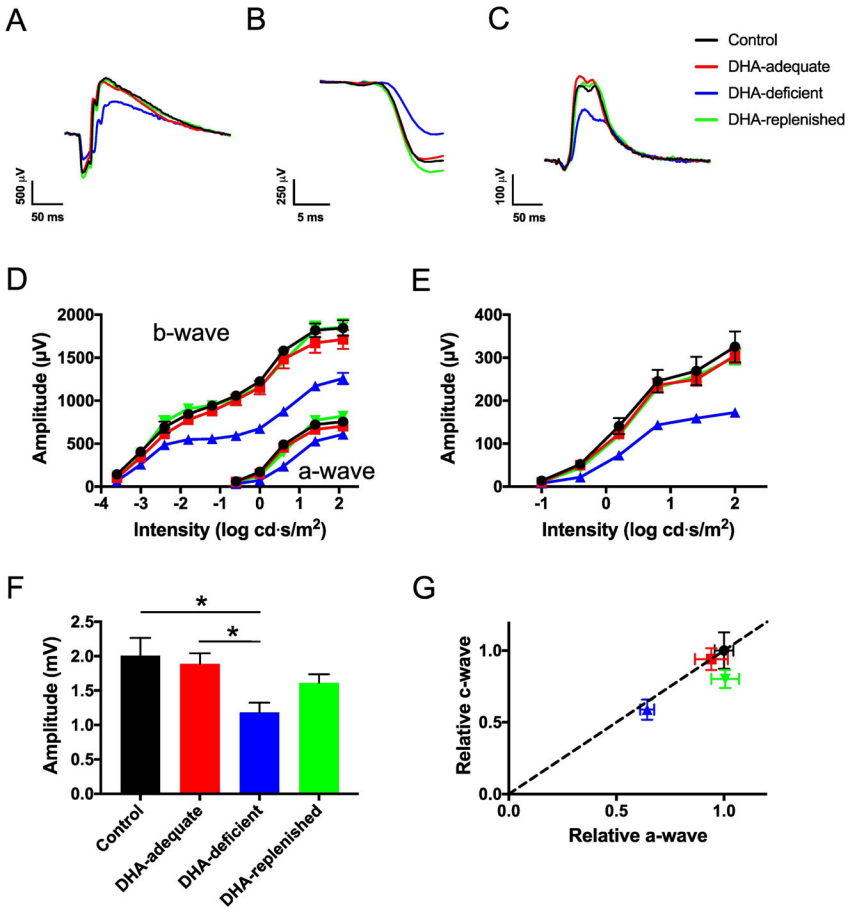

Fig. 1.

ERG performed on control (black, ●), DHA-adequate (red, ■), DHA-deficient (blue, ▲), and DHA-replenished (green, ▼) mice. (A) Representative ERG recordings obtained under scotopic conditions at a flash intensity of 24.1 cd·s/m^2. (B) Leading edge of the a-wave from traces presented in (A). (C) Representative ERG recordings obtained under photopic conditions at a flash intensity of 25.6 cd·s/m^2. (D) The a-wave and b-wave amplitudes obtained from scotopic ERG recordings plotted versus the intensity of the flash of light used to elicit the response. Significant differences ($p < 0.05$) from one-way ANOVA analysis were observed at each intensity of light for both a-wave and b-wave amplitudes. (E) The b-wave amplitudes obtained from photopic ERG recordings plotted versus the intensity of the flash of light used to elicit the response. Significant differences ($p < 0.05$) from one-way ANOVA analysis were observed at each intensity of light except the lowest intensity. (F) The c-wave amplitudes from ERG recordings obtained after administering a 5 cd/m^2 stimulus for 30 s. Significant differences ($p < 0.05$) from the Tukey's post-hoc test is indicated by asterisks. (G) A plot of relative c-wave versus a-wave amplitudes from ERG recordings obtained after administering a 5 cd/m^2 stimulus for 30 s. The dashed diagonal line indicates an equivalent change in a-wave and c-wave amplitudes. The means values are plotted with the standard error. The number of animals tested in (D) and (E) are as follows: control, $n = 4$; DHA-adequate, $n = 5$; DHA-deficient, $n = 6$; DHA-replenished, $n = 5$. The number of animals tested in (F) and (G) are as follows: control, $n = 4$; DHA-adequate, $n = 4$; DHA-

deficient, $n = 6$; DHA-replenished, $n = 4$. Details of statistical analyses are presented in Tables S2–S6.

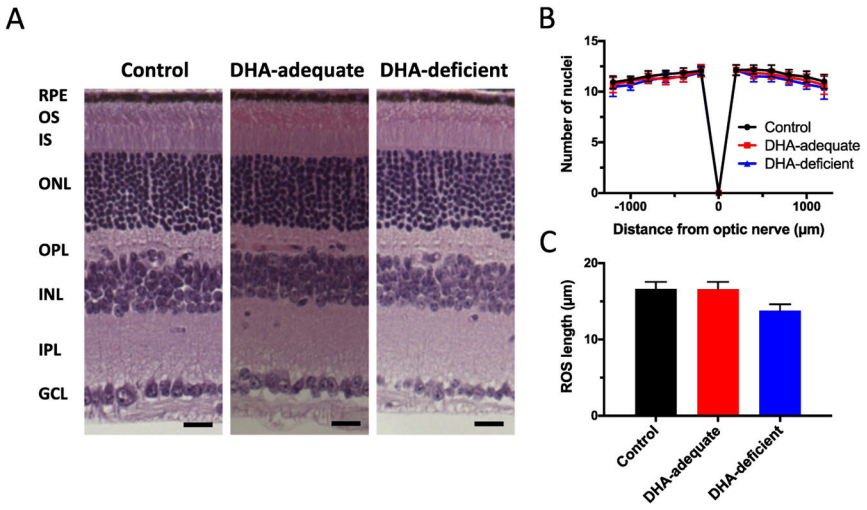

Fig. 2.

Histology of retina from control, DHA-adequate, and DHA-deficient mice. (A) Retinal sections are shown with the different layers of the retina labeled (RPE, retinal pigment epithelium; OS, outer segment, IS, inner segment, ONL, outer nuclear layer, OPL, outer plexiform layer, INL, inner nuclear layer, IPL, inner plexiform layer, GCL, ganglion cell layer). Scale bar, 25 μm. (B) The number of nuclei spanning the outer nuclear layer was determined in the superior (+) and inferior (−) regions of the retina. (C) The length of the ROS measured in retinal sections. Mean values are plotted along with the associated standard deviation. The number of mice (*n*) examined is 3. Statistical analyses of the data are presented in Table S7.

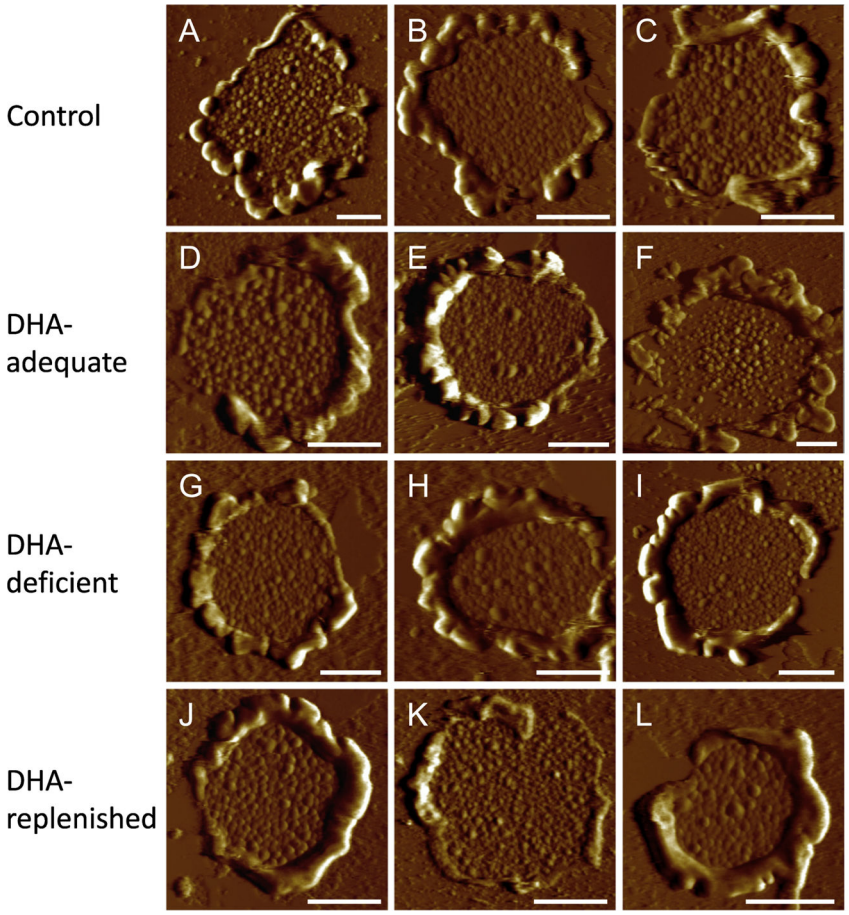

Fig. 3.

AFM images of ROS disc membranes. The deflection images are shown of ROS disc membranes from control (A–C), DHA-adequate (D–F), DHA-deficient (G–I), and DHA-replenished (J–L) mice. Scale bar, 500 nm.

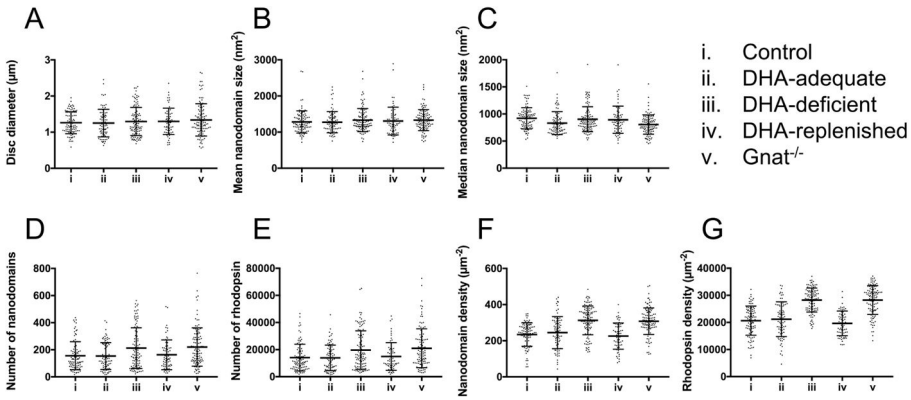

Fig. 4.

ROS disc membrane properties. ROS disc membrane properties are shown for control (i), DHA-adequate (ii), DHA-deficient (iii), DHA-replenished (iv), and *Gnat*$^{-/-}$ (v) mice. The mean values along with the individual data points are shown. Error bars represent the standard deviation. Statistical analyses of the data are presented in Tables S9 and S11. Data from *Gnat*$^{-/-}$ mice are those that were previously reported [38].

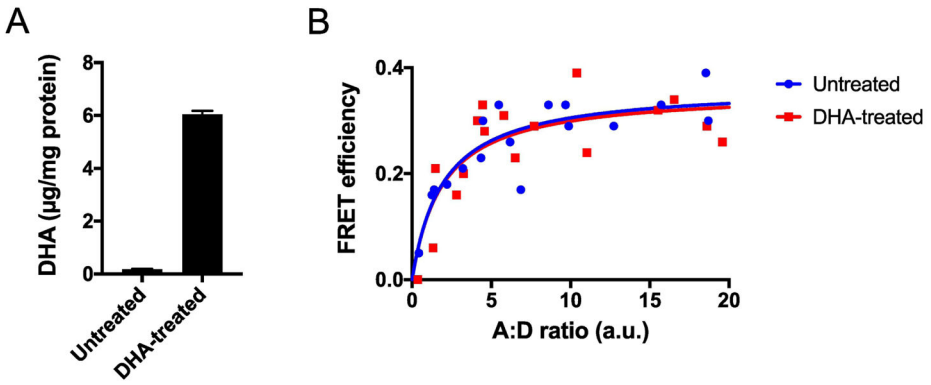

Fig. 5.

Impact of DHA on the oligomerization of opsin. (A) HEK293 cells were treated with 100 μM of the sodium salt form of DHA. The phospholipid DHA content in untreated cells was 0.18 ± 0.02 μg/mg protein (n = 3) and the amount in DHA-treated cells was 6.04 ± 0.14 μg/mg protein (n = 3). The mean and standard deviation are plotted. (B) FRET curves were generated by measuring the FRET efficiency at different ratios of SYFP- and mTq-tagged opsin (A:D). Plotted is the DM-sensitive FRET efficiency, which corresponds to opsin oligomers [50].

Table 1

DHA in the retina quantified by mass spectrometry

Mouse (*n* =4)	DHA (μg/mg of retina)	DHA (μg/mg protein)
Control	2.21 ± 0.27	30.45 ± 2.51
DHA-adequate	3.58 ± 0.19	46.11 ± 3.79
DHA-deficient	0.33 ± 0.03	3.99 ± 0.45
DHA-replenished	2.90 ± 0.62	35.79 ± 7.88
Gnat$^{-/-}$	2.20 ± 0.16	35.59 ± 0.93

DHA in membrane phospholipids was quantified by mass spectrometry as described in the Materials and Methods. Retina from control, DHA-adequate, DHA-deficient, DHA-replenished and *Gnat*$^{-/-}$ mice were examined and the number of mice examined is indicated by *n*. The amount of DHA is expressed either relative to the mass of the retina or total amount of protein. The mean values are reported along with the associated standard deviation. Statistical analyses of the data are presented in Table S1.

Table 2

Parameters from analyses of the ERG a-wave and b-wave

		Control (*n*=4)	DHA-adequate (*n*=4)	DHA-deficient (*n*=5)	DHA-replenished (*n*=4)
Scotopic a-wave	S ($ms^{-2}(cd{\cdot}s{\cdot}m^{-2})^{-1}$)	0.024 ± 0.003	0.019 ± 0.001	0.011 ± 0.001	0.018 ± 0.002
	Rm_{P3} (μV)	−744 ± 45	−726 ± 57	−626 ± 56	−772 ± 44
	t_d (ms)	2.08 ± 0.10	2.34 ± 0.04	2.56 ± 0.03	2.23 ± 0.10
Scotopic b-wave	K ($cd{\cdot}s{\cdot}m^{-2}$)	0.0029 ± 0.0011	0.0033 ± 0.0005	0.0012 ± 0.0002	0.0018 ± 0.0006
	R_{max} (μV)	1081 ± 29	1079 ± 33	581 ± 33	965 ± 43
	n	0.75 ± 0.10	0.67 ± 0.11	1.36 ± 0.14	1.09 ± 0.05
Photopic b-wave	K ($cd{\cdot}s{\cdot}m^{-2}$)	1.54 ± 0.09	1.55 ± 0.04	1.75 ± 0.10	1.56 ± 0.11
	R_{max} (μV)	284 ± 33	275 ± 14	190 ± 20	258 ± 10
	n	1.17 ± 0.06	1.24 ± 0.03	1.29 ± 0.02	1.25 ± 0.02

ERG traces obtained under scotopic and photopic conditions from control, DHA-adequate, DHA-deficient, and DHA-replenished mice were analyzed. The leading edge of the scotopic a-wave was analyzed by Eq. 1. Luminance response curves were generated for the b-wave and analyzed by Eq. 2. The mean values for each fitted parameter are reported along with the associated standard error. The number of mice examined is indicated by *n*. Statistical analyses of the data are presented in Table S5.

Table 3

ROS disc membrane properties

ROS disc membrane property	Parameter value			
	Control (*n*=95)	DHA-adequate (*n*=80)	DHA-deficient (*n*=108)	DHA-replenished (*n*=65)
Disc diameter (μm)	1.26 ± 0.30	1.25 ± 0.38	1.30 ± 0.39	1.30 ± 0.36
Mean nanodomain size (nm^2)	1281 ± 307	1274 ± 293	1331 ± 319	1306 ± 386
Median nanodomain size	920 ± 195	831 ± 212	903 ± 230	893 ± 251
Number (nm^2) of nanodomains	156 ± 103	154 ± 99	212 ± 150	163 ± 110
Number of rhodopsin	14105 ± 9882	13888 ± 9439	19619 ± 14205	14892 ± 10201
Nanodomain density (μm^{-2})	234 ± 65	245 ± 89	313 ± 80	226 ± 73
Rhodopsin density (μm^{-2})	20661 ± 5381	21195 ± 6417	28259 ± 4416	19661 ± 4558

ROS disc membrane properties are reported for control, DHA-adequate, DHA-deficient, and DHA replenished mice. The parameter values reported are mean values along with the associated standard deviation. The number of AFM images of single ROS disc membranes analyzed is indicated by *n*. Statistical analyses of the data are presented in Table S9.

Table 4

11-*cis* retinal content quantified by HPLC

Mouse	11-*cis* retinal (pmole/eye)
Control (*n* = 5)	398 ± 21
DHA-adequate (*n* = 3)	403 ± 19
DHA-deficient (*n* = 4)	427 ± 8

The amount of 11-*cis* retinal was quantified from the eyes of control, DHA-adequate, and DHA-deficient mice. The mean values are reported along with the associated standard deviation. The number of mice tested is indicated by *n*. Statistical analyses of the data are presented in Table S10.